Chapter 3 – THE CANONICAL CASES

3.1 AERODYNAMIC FORCE HISTORIES

We begin with a plot of lift coefficient histories for the eight cases, compared side-by-side as translation and rotation, plotted with the same time-base and axes definitions. The "fast" cases are plotted in two ranges of abscissa: one to emphasize the response when acceleration is non-zero, and a broader range (15 chords-traveled) to show long-term settling. The "slow" cases are all plotted with respect to 5 chords traveled. To reiterate, the rotations are with an AR = 2 plate with (primarily) 0.5 *c* root cut-out, while translations are with an AR = 4 plate. "Fast" pitch or surge has the acceleratory part occurring in a ramp linear with wall-clock time over 1 *c* of travel, while the "slow" cases do so over 6 *c*. The linear ramp is smoothed at its endpoints. Pitch motions begin with the plate at zero incidence and conclude with the plate at 45 degrees. Surge motions hold the plate at 45 degrees. Lift data are presented in two sequences; the first zooms in to early-time, emphasizing loads-history during the accelerated portion of the motion, and immediately thereafter. The second covers the entire recording-time, showing the long relaxation-transients after cessation of acceleration, in going towards the "steady-state" (or bluff-body shedding) response.

We first note the perhaps surprisingly good agreement between the various data sets, for each respective case. Occasionally there is an outlier, likely due to balance signal-to-noise reasons, tare-procedure and so forth (repeating a litany of possible experimental foibles is of nugatory value); often multiple curves mutually align, with one deviating, especially during the accelerated portion of the motion, but then later coming into mutual consonance. Figure 3-1 (translational case, left-hand side) is a typical case. This multi-way validation is encouraging, for it unifies the various data sets despite rather stark differences in types of model installation, blockage, Reynolds number and so forth. In particular, in some cases the plate is suspended vertically in a water tunnel or tow tank, with the load-cell atop of the water line, and the "tip" near the load-cell either piercing the free-surface or terminated with a splitter plate. In other cases the plate is mounted horizontally in the test section, supported by a sting aft of the plate, or midway along its pressure-side. The different kinds of blockage and physical obtrusions appear to not have any discernible major effect.

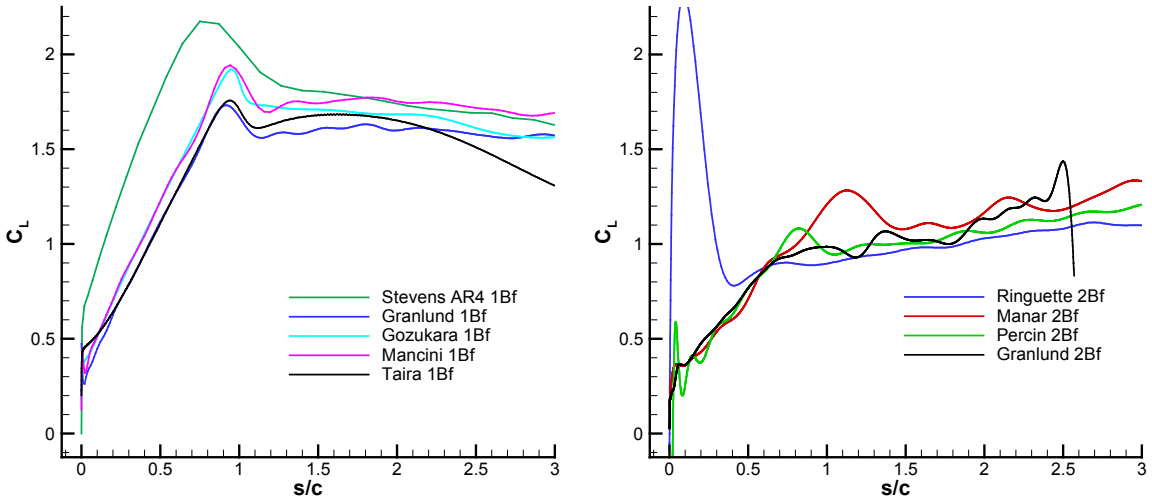

Figure 3-1: CL for the Fast Surging Cases. Translational (left) and rotational (right). Time-history through 5 chords of motion is shown. Note that data by Ringuette (right) is for a faster acceleration.

Next, we note the similarity in lift history reading across the row of each figure in this section – that is, comparing the translational and the rotational case. Members of each row are mutually more similar, than those of other figures. More precisely, translational pitch and rotational pitch resemble each other more, than do say translational pitch and translational surge. While the quantitative magnitude of force coefficients for rotation, and hence quantitative comparison with translation, depends on the choice of spanwise reference station in the defining an aerodynamic coefficient, the qualitative trends are unmistakable.

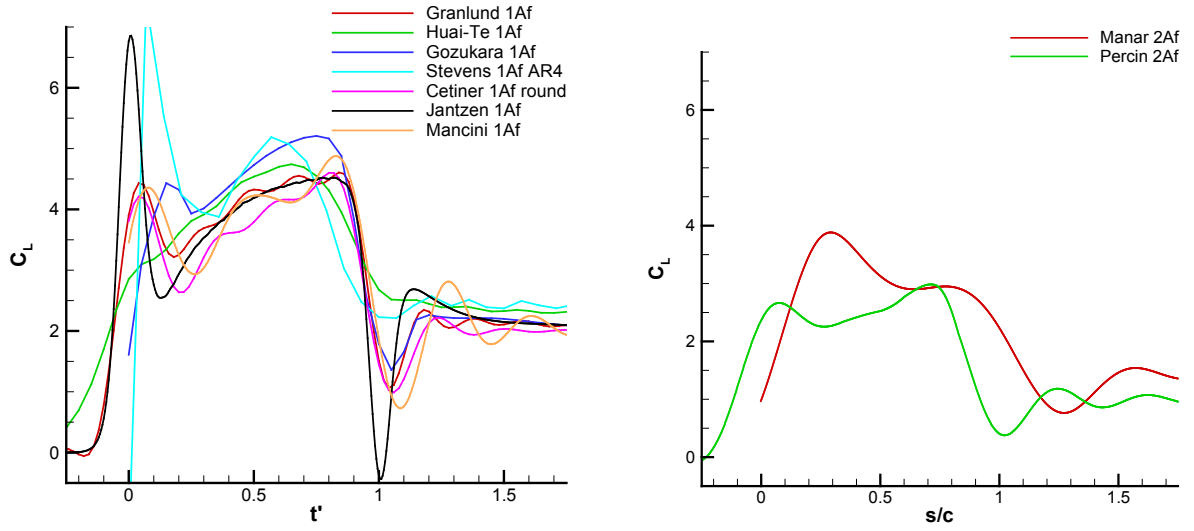

Figure 3-2: CL for the Fast Pitching Cases (LE Pivot). Translational (left) and rotational (right).

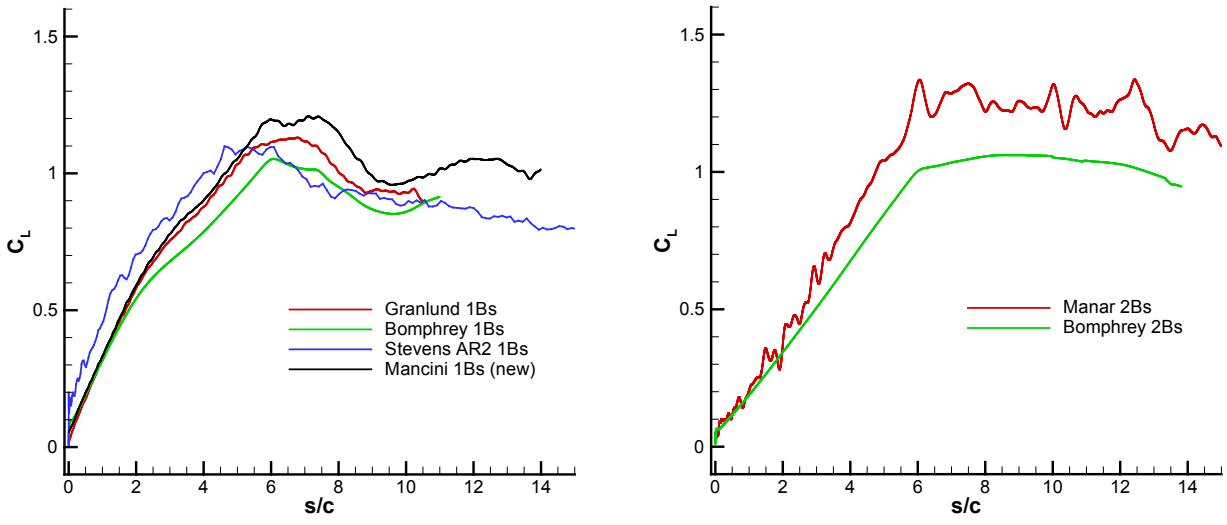

Figure 3-3: CL for the Slow Surging Cases. Translational (left) and rotational (right).

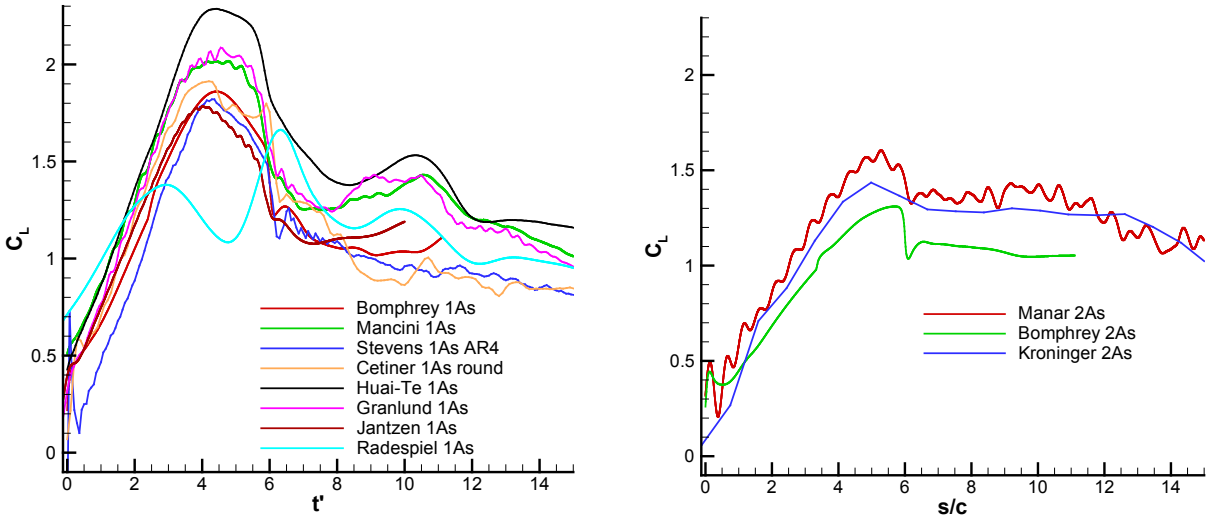

Figure 3-4: CL for the Slow Pitching Cases (LE Pivot). Translational (left) and rotational (right).

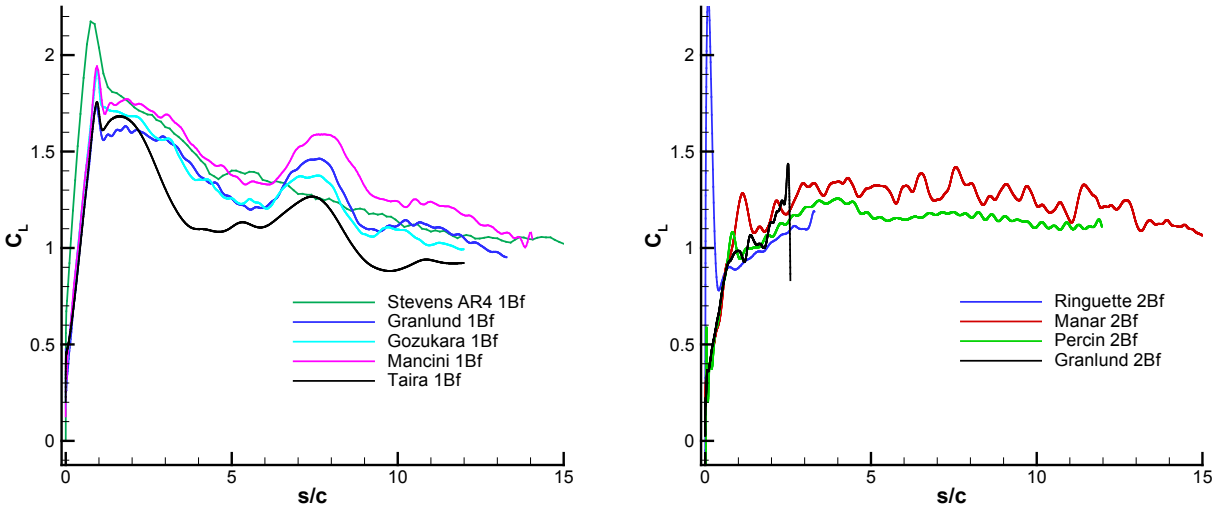

Figure 3-5: Long-Term History of CL for Fast Surging Cases. Translation (left) and rotation (right).

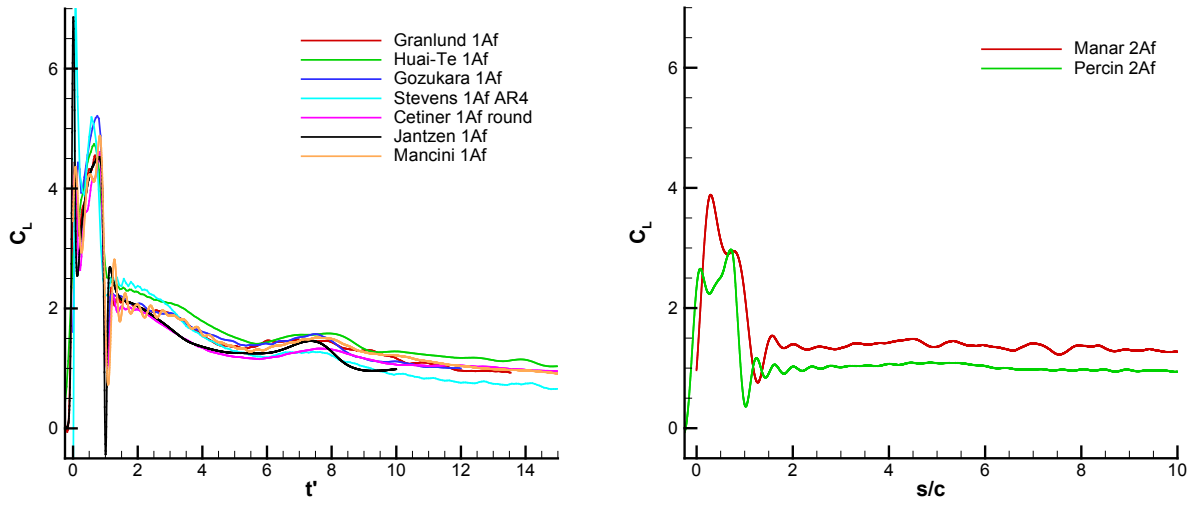

Figure 3-6: Long-Term History of CL for Fast Pitching Cases. Translation (left) and Rotation (right).

The long-term trend in all translational cases is evidently that it takes at least 15 chords-traveled for the effects of acceleration to completely dissipate, and for the lift history to asymptote to the "bluff body shedding" or quasi-steady-state. This is true whether the acceleration was "fast" (1 *c*) or "slow" (6 *c*). The rotational cases are different: there the lift response reaches a more or less constant value after 5 *c* of travel, or less. Instead of a long and slow relaxation, there may be a rise in lift after the accelerated portion of the motion is over, followed by a long steady period. In some cases, the wing revolves through its own way, and depending on the blockage of the installation (distance between wing tips and walls of the tank [44]), lift history declines slightly after a full revolution has been completed.

We next turn to the drag histories, this time for all 8 cases plotted across 15 convective times, again with translation on the left-hand side, and rotation on the right-hand side.

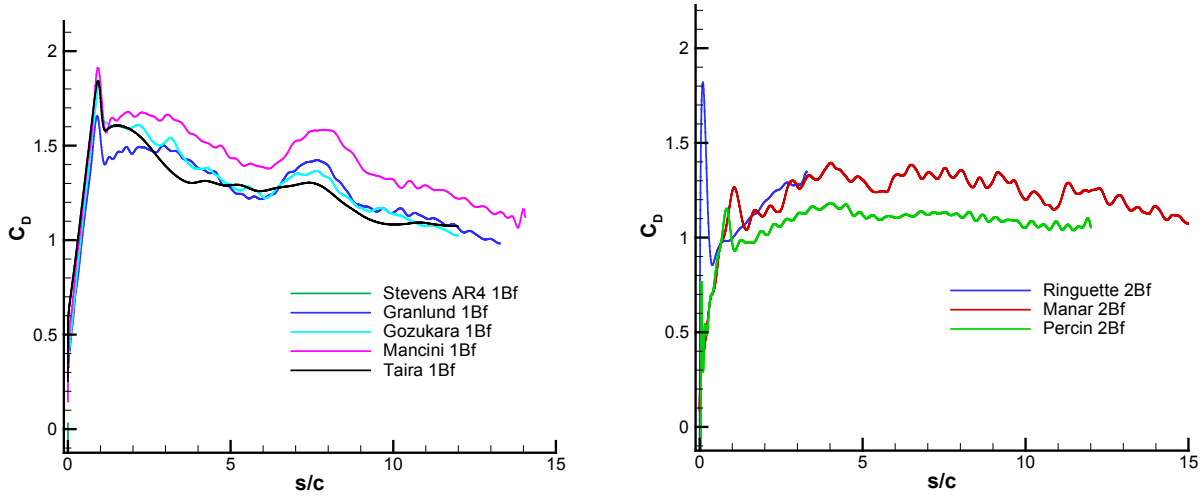

Figure 3-7: CD for the Fast Surging Cases. Translational (left) and rotational (right).

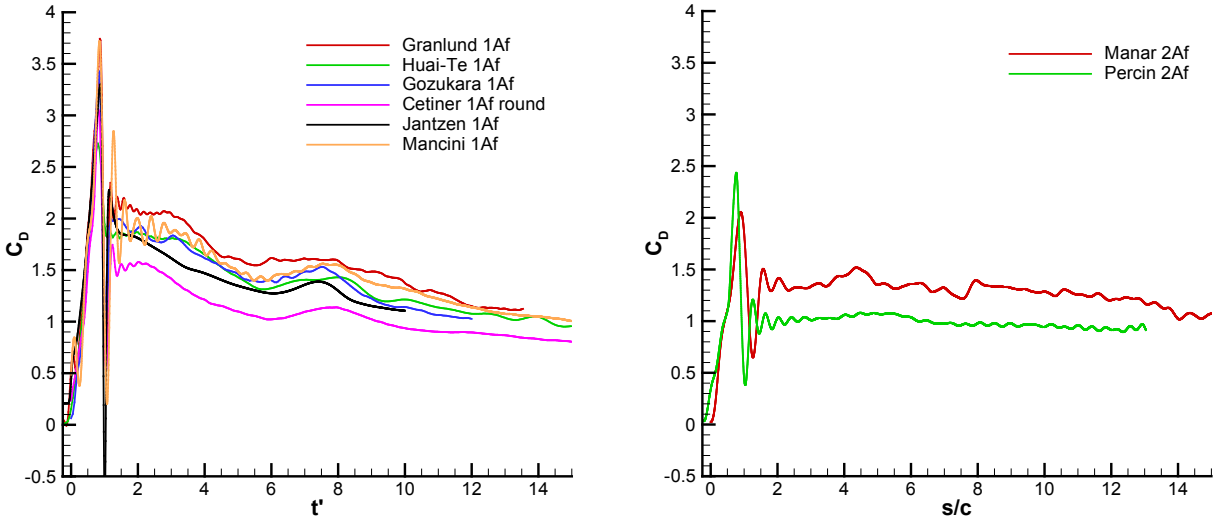

Figure 3-8: CD for the Fast Pitching Cases. Translational (left) and rotational (right).

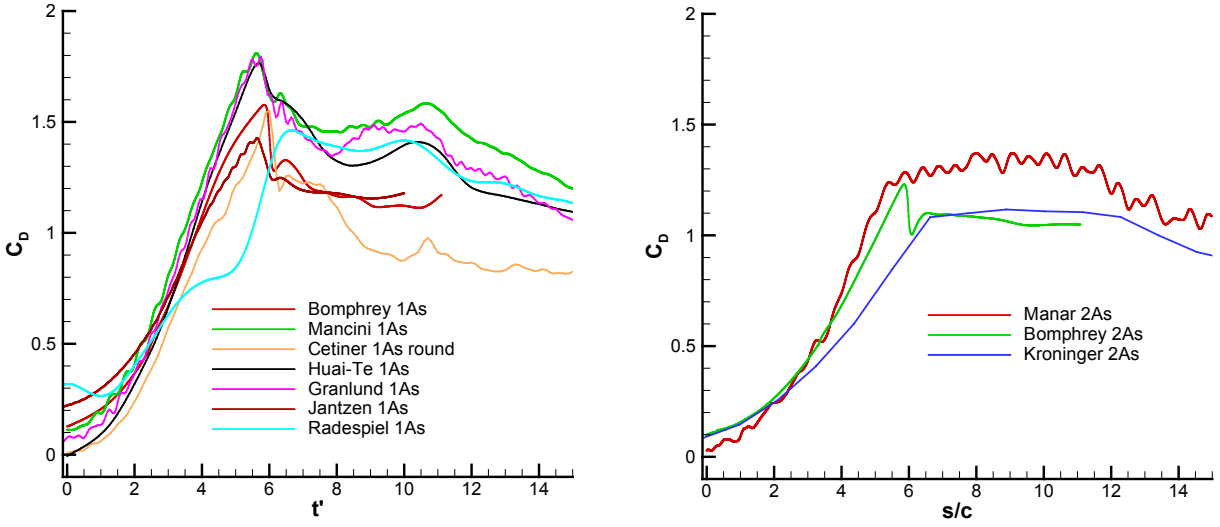

Figure 3-9: CD for the Slow Pitching Cases. Translational (left) and rotational (right).

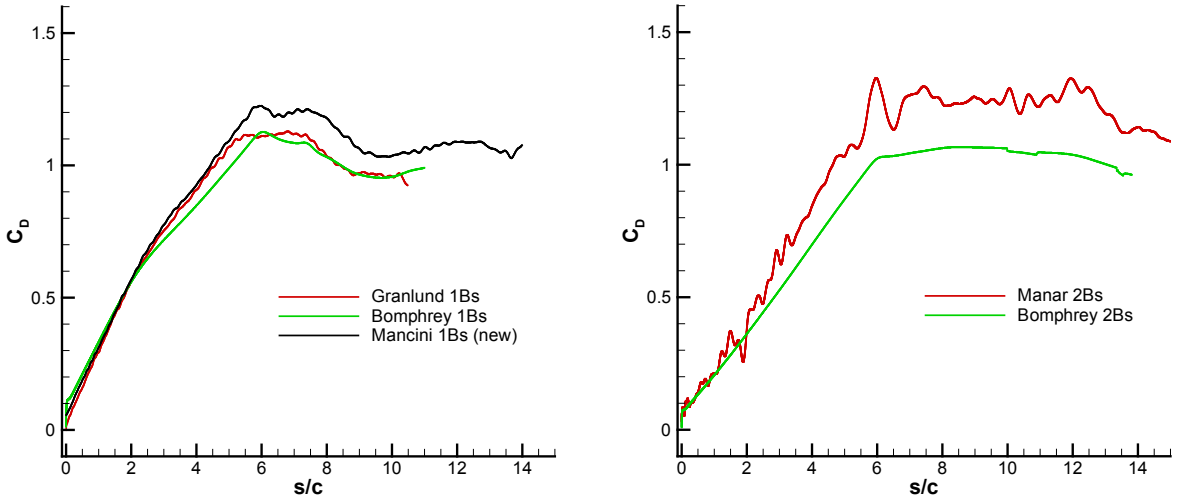

Figure 3-10: CD for the Slow Surging Cases. Translational (left) and rotational (right).

Importantly, for the surging cases (rotational or translational, fast or slow), the lift and drag histories resemble each other very closely. This is not surprising, as the net aerodynamic force is essentially plate-normal, and the plate is at 45 degrees incidence. For the pitching cases the situation is rather different; lift tends to be larger than pitch during the accelerated portion of the motion, or in other words, L/D > 1. Thus pitch has a double aerodynamic benefit over surge: it produces a net larger force, and a net higher L/D.

3.2 LEADING EDGE AND TRAILING EDGE VORTEX STRENGTHS AND TRAJECTORIES

Figure 3-11 shows the LEV circulations measured by a variety of groups for the fast pitch and surge cases. Before discussing this result in detail the following should be noted:

- The methods of determination of vortex strengths vary widely between groups and are subject to considerable error. In the slow case the LEV is not very distinct and this has made it impossible to distinguish any trends in circulation growth.
- Sometimes, neighboring secondary vortices become included in the calculation of LEV strength – this can cause sudden steps in the circulation distribution.
- The circulation data is non-dimensionalised by a Γ_∞ which is equivalent to $c_L = 2\,\pi\alpha$, with $\alpha = 45°$. Thus, the non-dimensional circulation shows how the LEV strength compares to an assumed steady-state thin airfoil theory bound circulation.
- The data are compared to a Wagner function which also asymptotes at a non-dimensional circulation of unity.

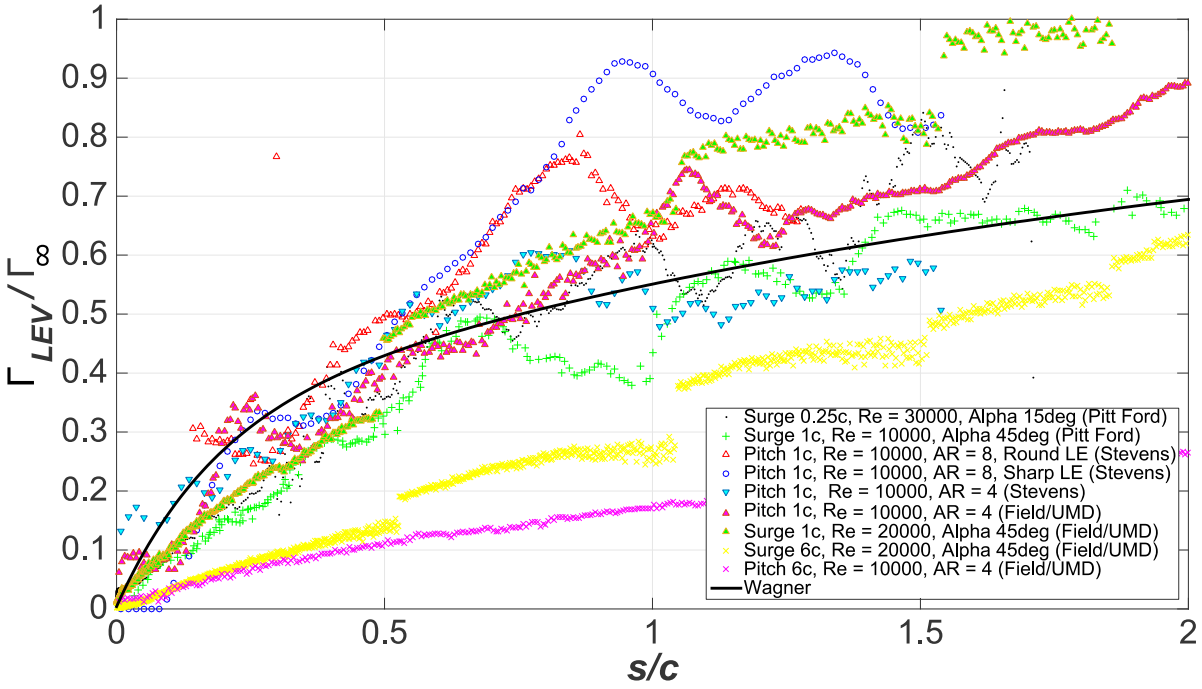

Figure 3-11: Collection of Normalized LEV Circulation Histories from Various AVT-202 Contributors, for Translational Pitch and Surge Cases; Compared with Wagner's Theoretical Curve [53].

The difficulties in vortex strength determination are clearly reflected in the data. Overall the scatter between different groups is far larger than the differences between different cases. Also, the scatter becomes noticeably larger with time. This is a reflection of the break-up of the initially coherent LEV and the appearance of secondary vortices. Nevertheless, ignoring some obvious outliers, there are some clear trends.

Somewhat surprisingly, there are no obvious differences between pitch and surge. As a rough approximation all data follows the Wagner function reasonably well. During the early part of the motion the Wagner function slightly over-predicts vortex strength. This can be interpreted as a reflection of the fact that during this part of the motion the wing is not yet at either the final velocity or angle of attack. Thus one might expect that the equivalent 'asymptotic Wagner value' to be lower.

To account for the reduced strength of the vortices early in the cycle, Figure 3-12 shows the data for the fast pitch and surge cases with a Wagner function that has been modified for $s/c < 1$ by the equivalent angle of attack or free stream velocity (or, in other words, by multiplying the original Wagner function with a linear ramp). It is debatable whether this fit is better than the original unmodified Wagner function, although the actual shape of the vortex growth is somewhat better reflected. Either way, given the large amount of scatter in the experimentally determined LEV circulations it is proposed to adopt the Wagner function (modified or unmodified) for the low-order model calculations. This is certainly the only viable route for the calculation of the vortex growth term as the experimentally data are too noisy to allow a meaningful calculation of $\dot{\Gamma}$.

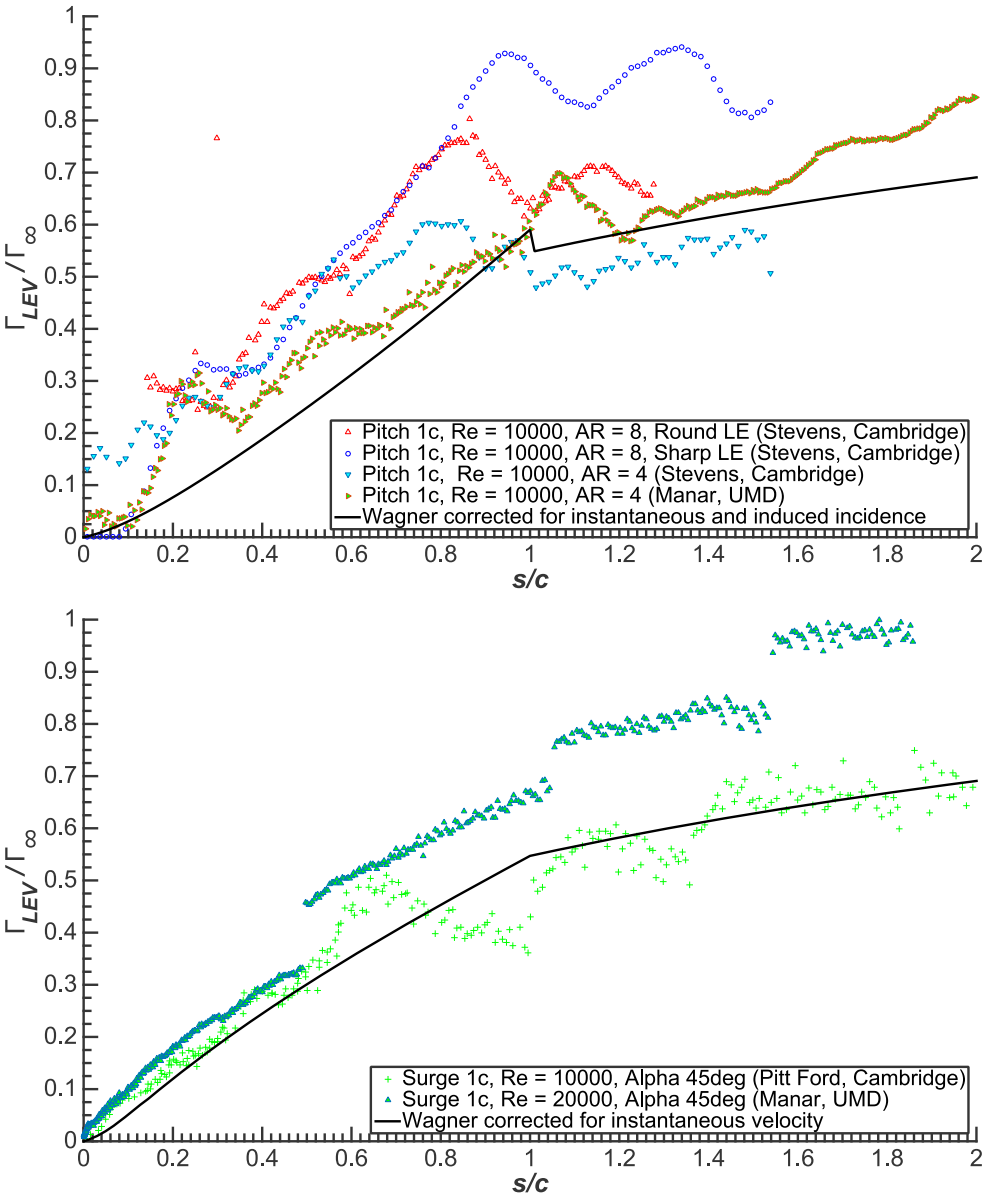

Figure 3-12: Normalized LEV Circulation Compared to 'Modified' Wagner Function for Pitch (Top) and Surge (Bottom). Note the small kink in 'Wagner' circulation in the pitch case as a result of the induced angle of attack during the pitching motion.

Similar difficulties with the vortex detection schemes affected the determination of vortex trajectories. Figure 3-13 shows the distance (in chord-lengths) between the detected LEV center and the plate leading edge for the fast pitch case through the first three chord lengths of motion. Given the measurement difficulties it is impressive how well the various datasets collapse. Overall the relative speed between the LEV and the plate is approximately $\frac{1}{3}U_\infty$.

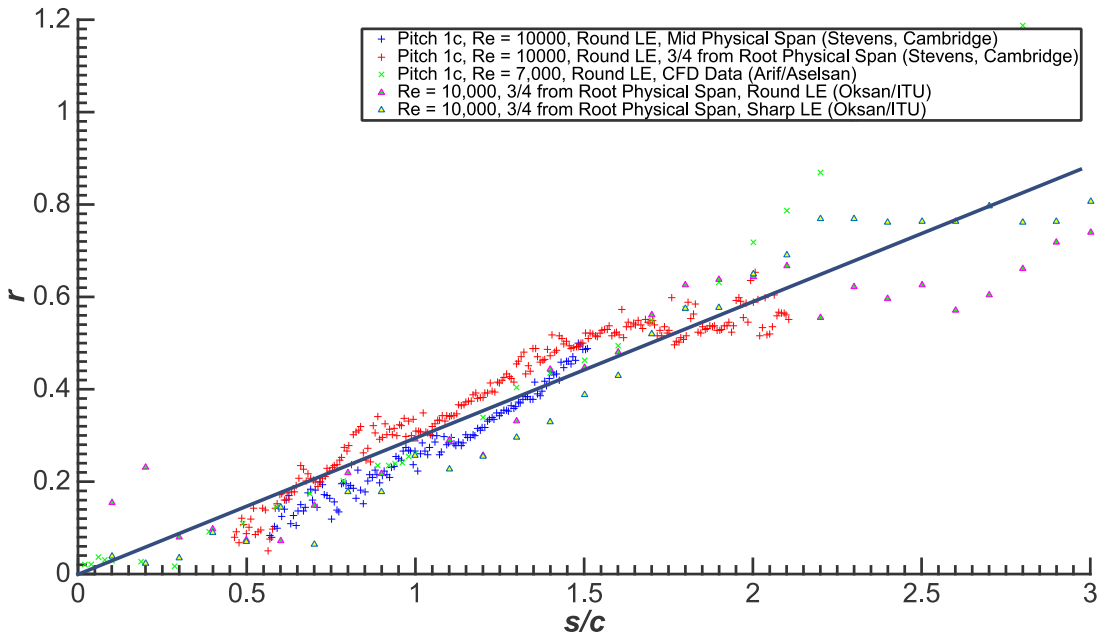

Figure 3-13: LEV Distance from Plate Leading Edge for the Fast Translational Pitch Case.

Figure 3-14 compares leading and trailing edge vortex trajectory data for the translational pitch and surge cases, as measured in the Cambridge University towing tank. The LEV trajectory is again very similar and follows the same trend (of $\frac{1}{3}U_\infty$) while there are clear differences in the TEV behavior. It appears that the TEV formation is delayed in the pitch case: it cannot be detected until the wing has travelled almost half a chord length. Thereafter the TEV moves away from the wing faster than in the surge case (although it has to be kept in mind that the surging wing has not yet reached full speed at this point). Ultimately however, both TEV trends converge onto the same line which suggests that the TEV reaches something around 80% of U_∞ by the end of the acceleration period. Thus, it can be suggested that a good model for the *relative* velocity between the TEV and the LEV during the unsteady part of the motion is 50% of U_∞ for the pitching wing and 0.3 U_∞ for the surging wing. Thereafter 0.3 U_∞ appears to fit both cases reasonably well.

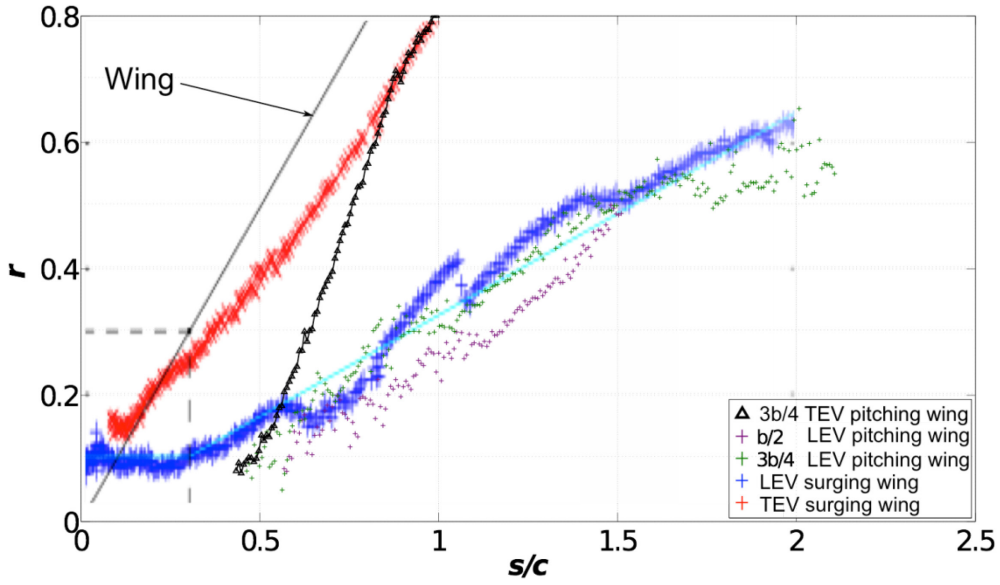

Figure 3-14: LEV and TEV Distance from Leading Edge for Fast Translational Surge and Pitch Case (Data from Cambridge University Group). 'Wing' indicates the trajectory of an object moving away at U_∞.

3.3 EVOLUTION OF VELOCITY AND VORTICITY FIELDS

Because a low-order model is used to estimate aerodynamic loads, and not a whole flowfield integration [8], velocity field data is more for illustrative purposes, than for quantitative calculation. The idea is to qualitatively relate LEV, TEV and tip vortex development to the history of lift and drag. In some cases we compare qualitative and quantitative visualization; that is, dye concentration vs. measured or computed vorticity.

3.3.1 Translational Pitch and Surge

LEV and Tip Vortex (TV) development during pitching is given in Figure 3-15(a), (c), (e) and (g); the left-half of the page is for the fast case, and the right-half is for the slow case.

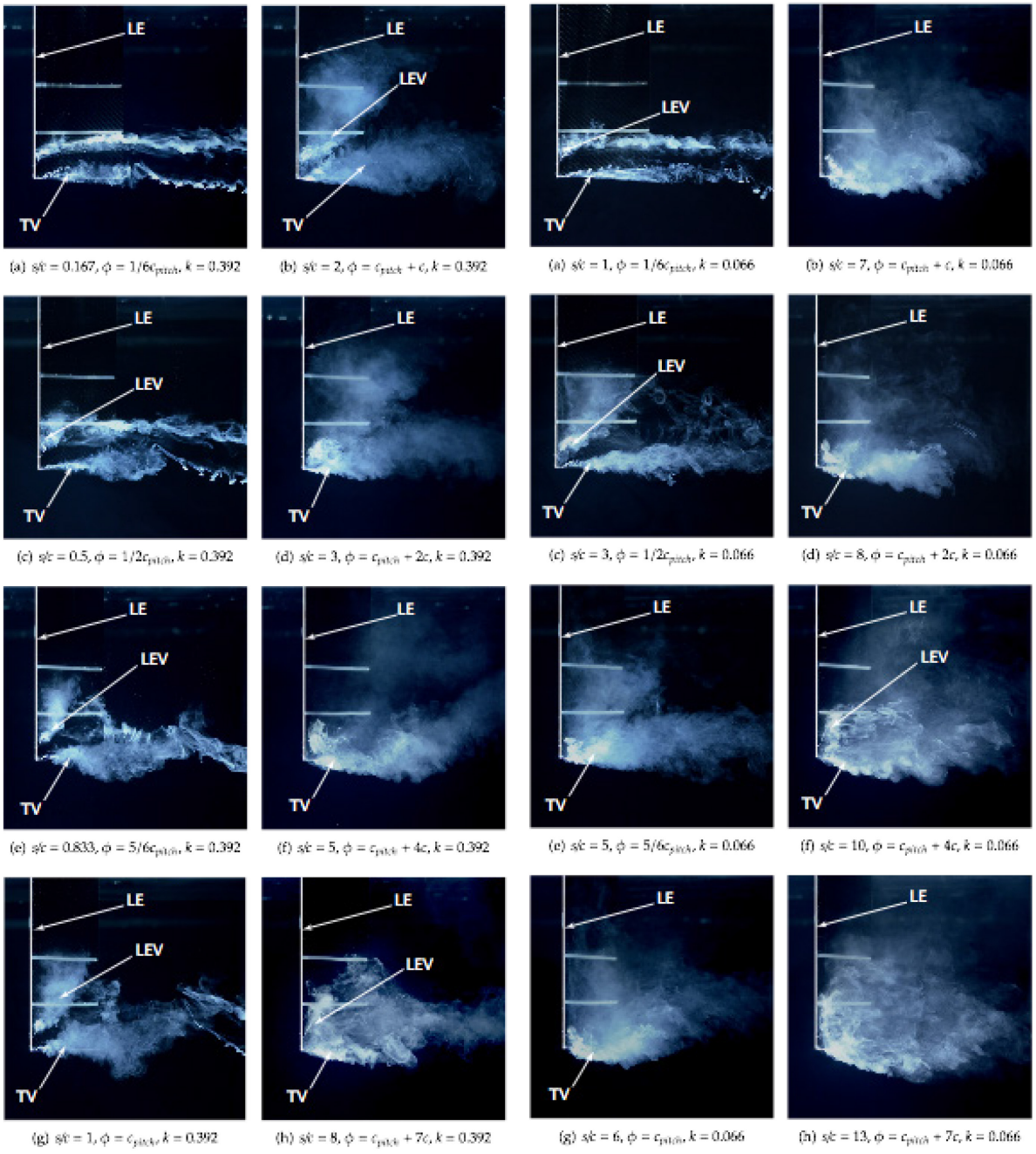

Figure 3-15: Case 1a, Translational Pitch, LEV/TV Interaction Flow Visualization; Eight Images on Left are for the Fast Case (1 chord pitch), and Eight Images on the Right are for the Slow Case (6 chords pitch). Instances of chords-traveled as marked, progressing sequentially for the fast case down the first column of the figure, then the second column; and for the slow case down the third column of the figure, and then down the fourth column.

We first consider the pitching fast-case. Initially, the flow is attached with little discernible tip influence at s/c = 0.167. By s/c = 0.5 a clear and distinct LEV and TV are beginning to form, but with no obvious interaction.

As the incidence angle increases (s/c = 0.833 and s/c = 1) the TV grows concurrently with the LEV. The angle between the distinct LEV and TV from the LE and tip apex is approximately 45°. The downwash from each vortex will superimpose here, and this mechanism may point towards a physical reason as to why the LEV remains more coherent closer to the wing tip. During the translation part of the motion (Figure 3-15(b), (d), (f) and (h)), the dye disperses as the LEV and TV grow. By s/c = 5, the dye from the LE is fully entrained into the tip vortex and by s/c = 8 we see the beginning of the reformation of an LEV type structure in the outer span region of the wing, albeit a much less defined structure than that which manifested while pitching occurs.

Turning to the slow pitching case (right-hand side of Figure 3-15), initially the flow evinces small and well-defined TV and LEV. By s/c = 3, the TV has developed but remains coherent, whereas the LEV is weak and only has a coherent form close to the tip. At s/c = 5 the LEV has dispersed, and by s/c = 6, the tip vortex is the dominant structure. After cessation of pitching motion, the flow is largely separated, with the exception of the reformation of a small LEV-type structure at s/c = 10. Comparing again with the lift coefficient history, we gain some physical insight and propose that the presence of a weak LEV/weak circulatory flow is intrinsically linked to an increase in streamline curvature, and is therefore responsible for an increase in the force.

We now turn to an alternative presentation of the fast pitching case, as an isometric view of sectional visualizations. Fluorescent rhodamine dye injection illuminated by a planar light sheet is compared with black and white rendition of computed vorticity contours in Figure 3-16. Evidently a "suitable" value of normalized out-of-plane vorticity value renders the quantitative vorticity information looking very similar to the qualitative dye-concentration information.

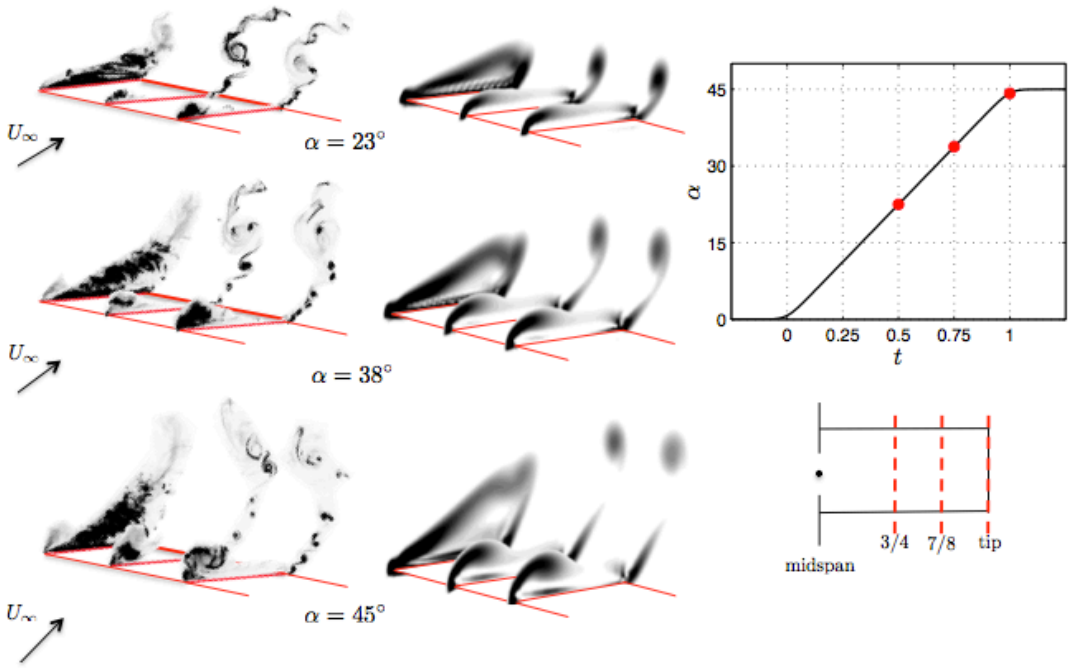

Figure 3-16: Juxtaposition of Flow Visualization by Planar Laser Illumination of Fluorescent Dye in a Water Tunnel at Re = 20,000 (Left Column) and Black and White Rendition of Spanwise Vorticity Contours from Direct Numerical Simulation at Re = 300 (Middle Column) for the Fast Translational Pitching Case. Instances of flow evolution along the motion-history as marked, visualized at the 3/4 span, 7/8 span and tip locations.

Figure 3-17 compares the fast pitch, fast surge, slow pitch and slow surge at instances of chords-traveled of 0.5, 1.0, 1.5, 2.5, 3.0, 5.5 and 8.0. These are 2D PIV images at the ¾-span location. Evidently, the fast cases evince a more compact and more coherent LEV. The fast pitch and fast surge have similar LEV developments. Their respective TEVs differ in that the pitching-case has fully-developed free-stream speed at all times, whence the TEV convects rapidly from the plate's TE, whereas in the surging case the plate accelerates away from its TEV in accordance with its surge history; that is, the TEV is essentially stationary in the lab-frame. The slow pitching case has a delayed LEV development, with a reasonably coherent LEV present even at s/c = 3, whereas in both fast cases the LEV has lifted off and evidently saturated. However, at s/c = 5.5 in the fast cases a second LEV appears to be forming, whereas in the slow pitch the initial LEV still lingers more or less. Unfortunately only a limited data set is available for the slow surge (fourth column of Figure 3-17). At s/c = 1.0, the overall flow topology of the slow surge much resembles that of the fast surge, albeit the LEV strength is evidently reduced for the slow case. The comparability persists through s/c = 2.5, which is the last frame for the slow surging case for which data are available. In short, the outlier in terms of gross flowfield features is the slow pitching case.

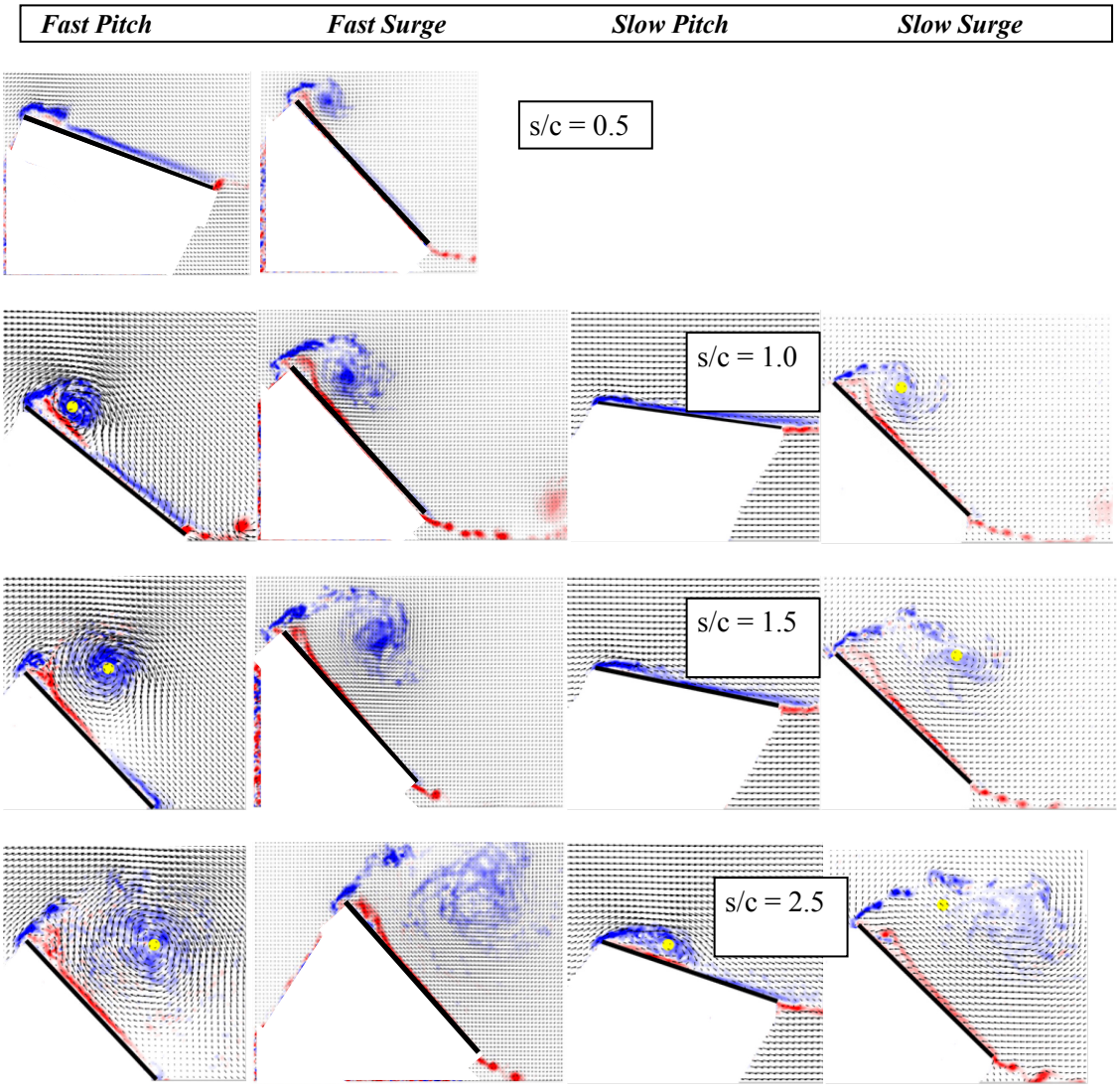

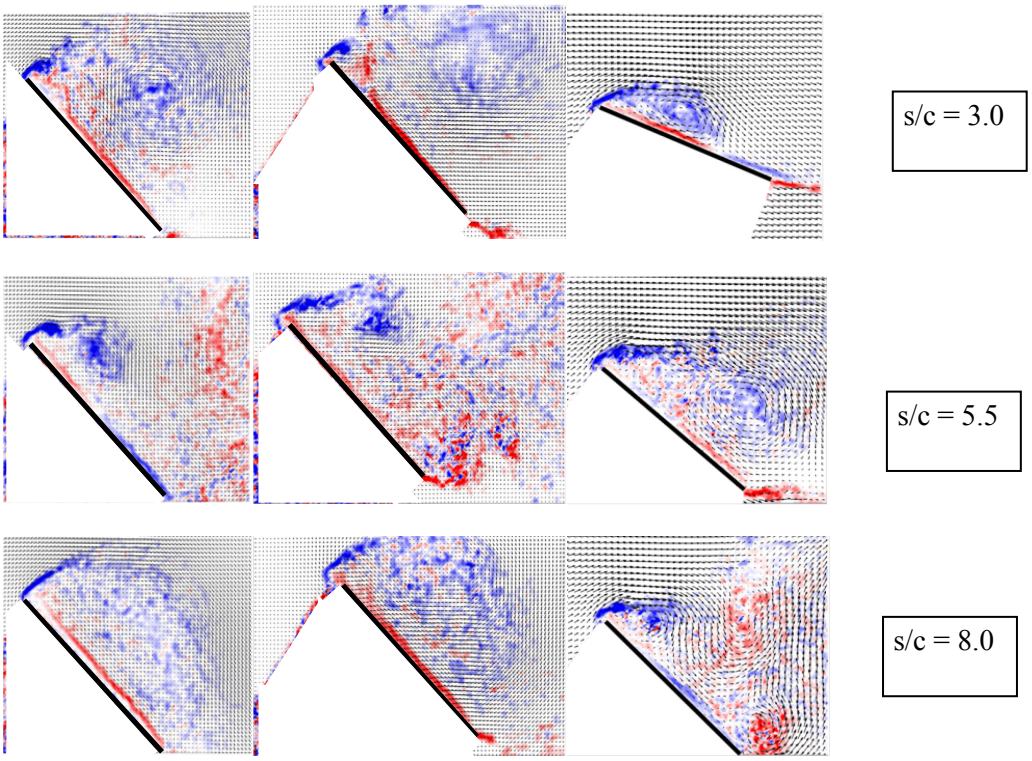

Figure 3-17: Frame-by-Frame Comparison of the Four Translational Cases, AR = 4 Plate, ¾-Span Location, with PIV-Derived Vorticity and Velocity; Time-Instance as Marked in Each Row.

3.3.2 Rotational Surge

Figure 3-18 follows the rubric of Figure 3-17 in rending sectional flowfield ensemble-averaged PIV results for the slow and fast rotational surge cases. In Figure 3-18, snapshots are arranged by azimuthal angle traversed by the plate, with conversion given from this angle to an "equivalent" arc-length. This length is normalized by chord, taken at the 15c/8 location spanwise along the plate, from the point of rotation. The reason for 15c/8 is that with 0.5 *c* root cut-out (that is, distance between the point of rotation and the inboard wingtip of 0.5 *c*), a distance of 15c/8 from the point of rotation is at 75% of the distance to the outboard wingtip [13].

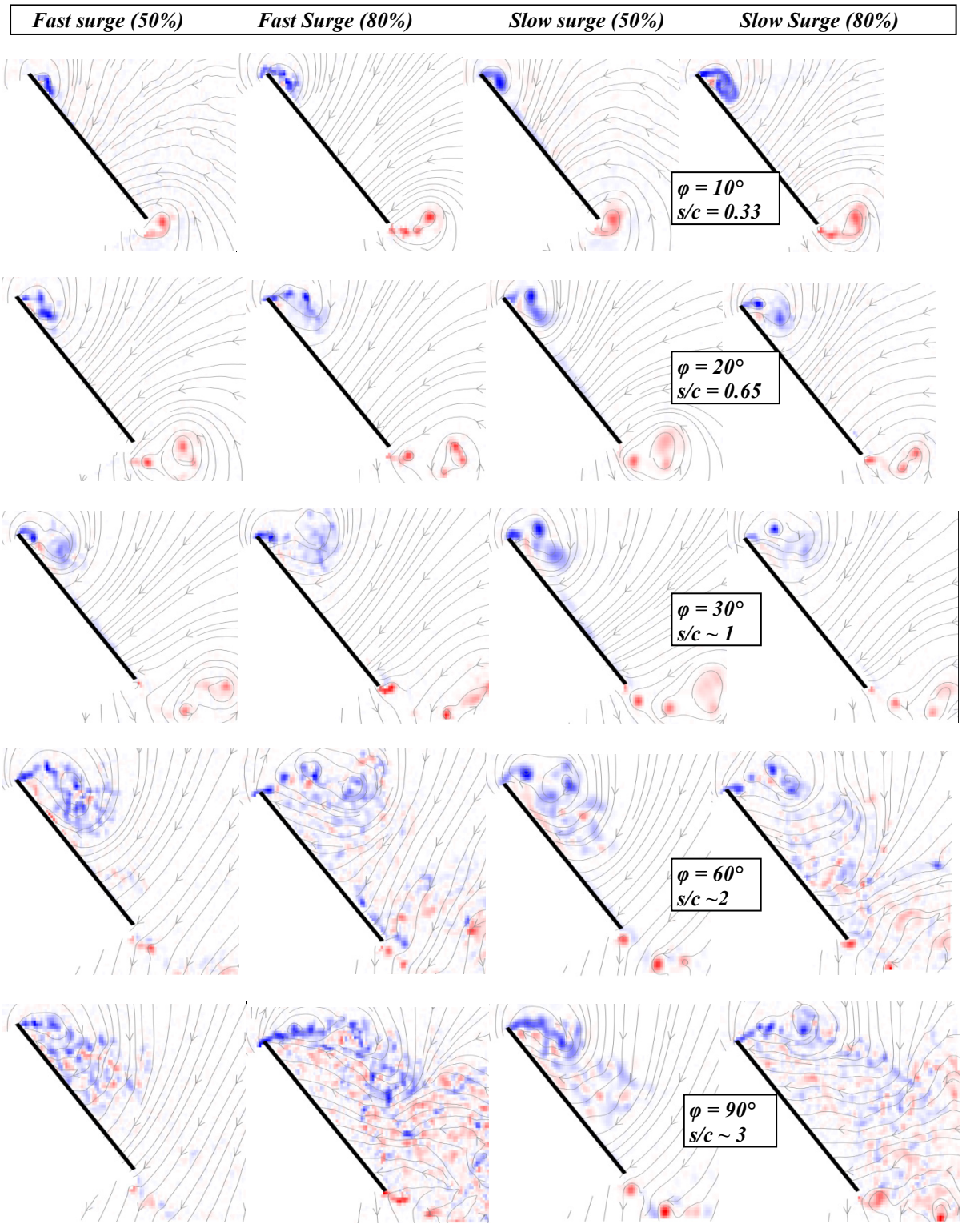
Fast surge (50%)
Fast Surge (80%)
Slow surge (50%)
Slow Surge (80%)
φ = 10°
s/c = 0.33
φ = 20°
s/c = 0.65
φ = 30°
s/c ~ 1
φ = 60°
s/c ~2
φ = 90°
s/c ~ 3

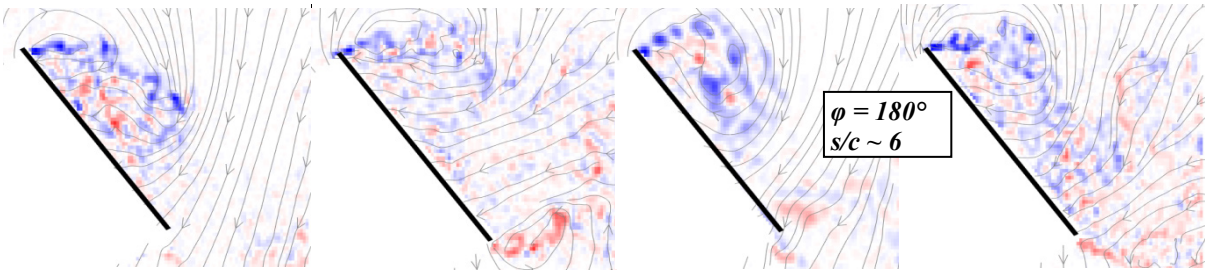

Figure 3-18: Tableau (Phase-Averaged PIV Vorticity Contours and Projected Streamlines, University of Maryland Group) of Rotational Surge Cases. Columns, left to right: Fast surge, 50% spanwise location (which is to say, at the midspan); Fast surge, 80%; Slow surge, 50%; and finally Slow surge, 80% spanwise location. Rows, top to bottom, are by degrees of azimuthal rotation at the snapshot, starting from rest: 10, 20, 30, 60, 90 and 180. This is equivalent to chord-normalized distance traveled (compare to Figure 3-17) of s/c = 0.33, 0.65, 1, 2, 3 and 6, respectively.

Two spanwise locations are given: 50% (the midspan) and 80% (that is, near the outboard tip). For all 50% images, whether the motion is "fast" or "slow", one sees in the aggregate a coherent LEV. Its constituent parts are not of one simply-connected, single-signed agglomeration of vorticity, evidently owing to vortex breakdown [47], but a vortex is nonetheless discernable without excessive recourse to poetic license. At the 80% spanwise location this is not the case. However emanates the leading edge shear layer, it does not appear to curve around towards the suction-side of the plate, and by s/c ~ 6 there is dead-water region on the plate's suction-side. Evidently, if there is stable LEV, it has curved around into the streamwise direction and has lifted off of the plate's suction side. More of this is discussed in 3D in the section on incidence-angle variations.

3.3.3 Rotational Pitch

Flowfield data on rotational pitch are not available from amongst the research-groups mentioned in the previous chapter. The reader is referred to Bross and Rockwell [15] for comparison of 3D PIV-derived flowfield measurements between rotational surge and rotational pitch.

3.4 APPLICATION OF THE LOW-ORDER MODEL

Having surveyed the measured/computed aerodynamic force history, vortex trajectories and the flowfield evolution, we now combine all three conceptual modalities to compare the modeled lift history for the translational cases with the measured/computed, where the model is predicated on:

1) Simple models of the vortex growth and motion (as discussed earlier); and
2) The assumption that in early-time the flow is acceptably two dimensional.

Thus, we have not applied the model to any of the rotational cases, although it remains to be seen whether a suitable 'strip-theory like' approach can yield some success.

3.4.1 Fast Surge Case

First we concentrate on the surging wing. In line with the observations discussed earlier we make the following assumptions:

1) The LEV grows as predicted by a Wagner function, albeit moderated during the acceleration phase by the instantaneous velocity $(t)/u_{\infty}$.
2) The relative motion between the LEV and the TEV is set to 0.3 U_{∞}.
3) The distance between any newly formed additional LEV circulation and its TEV counterpart is one chord length (to be used in the 'vortex chord term').

Finally, the sum of all force contributions is smoothed to approximate typical experimental filtering of force data (although the level of numerical smoothing is still relatively small).

Figure 3-19 shows the result of the model and its individual contributions, compared to a notional experimental dataset; both are from the Cambridge group. The overall curve displays the familiar initial peak with a relatively quick return to some sort of steady-state value after the acceleration period. Further insight is gained by studying the individual force contributions. The main contributors to the initial force peak are the added mass and vortex growth terms. Thus we can see that for this motion the LEV growth is indeed a dominant factor in the lift generation, albeit enhanced by the non-circulatory term. Later on in the cycle the 'vortex motion' term dominates, thus taking the role of some sort of 'bound' circulation produced by the wing (although the LEV drifts away from the wing it nevertheless contributes a fair amount of lift). Interestingly, the decaying vortex 'vortex growth' term added to the asymptotically growing 'vortex motion' term gives an almost constant overall force in the post-acceleration phase. Throughout, the 'vortex-motion' term closely resembles the modified Wagner function (as it should since the relative velocity is assumed to be constant throughout) and thus the effect of the initial 'moderation' during the acceleration phase is seen clearly. It turns out that the exact kinematics during the acceleration phase have a significant impact, because the 'vortex growth' term depends strongly on the shape of the circulation growth curve. This is illustrated by an alternative application of the model from the Maryland group for the same test case, as shown in Figure 3-20.

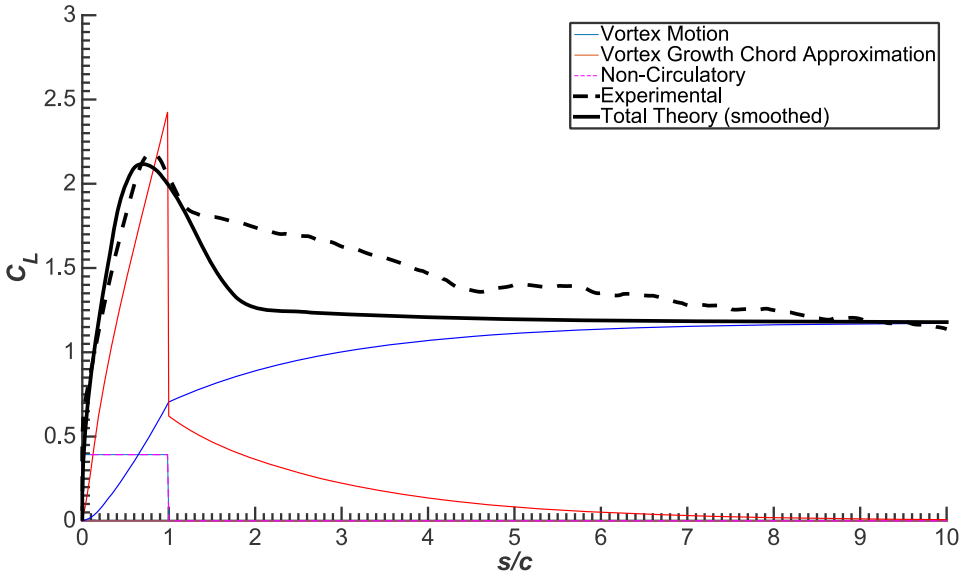

Figure 3-19: Low-Order Model Prediction for the Fast Surge Case (Data from University of Cambridge Group).

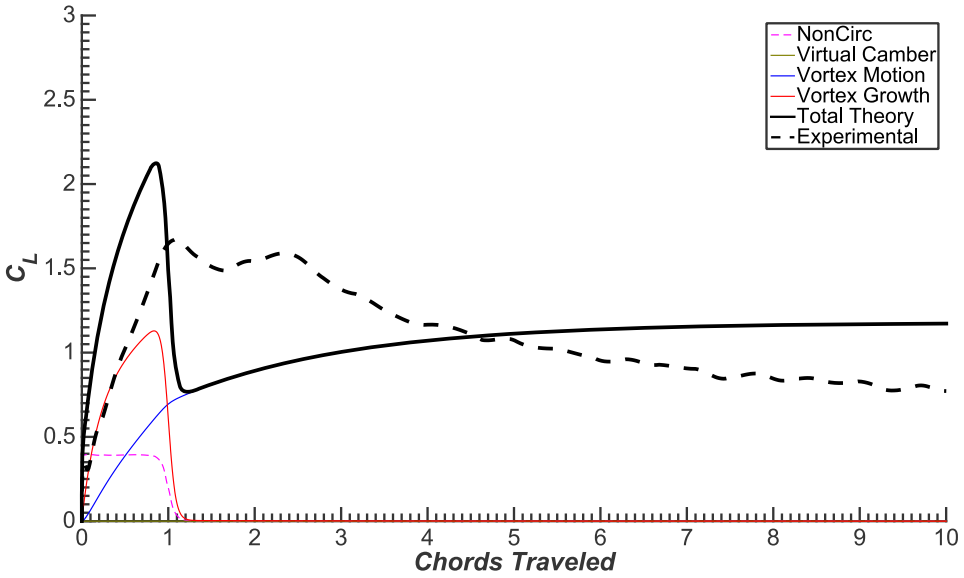

Figure 3-20: Variation on Figure 3-19, from the University of Maryland Group.

In Figure 3-20, a slightly different 'moderation' is applied to the Wagner function, and the resulting 'vortex growth' term has a rather different shape and magnitude, fitting less well with the experimental data. Note that there is a slightly non-standard implementation of the 'vortex growth' term, which also introduces some discrepancies during the constant-speed part of the motion.

Another sensitivity of the model is the relative LEV-TEV velocity. Figure 3-21 compares model predictions for two different relative velocities, 0.3 U_∞ and 0.5 U_∞. There is a considerable difference in the 'steady-state' portion of the model prediction.

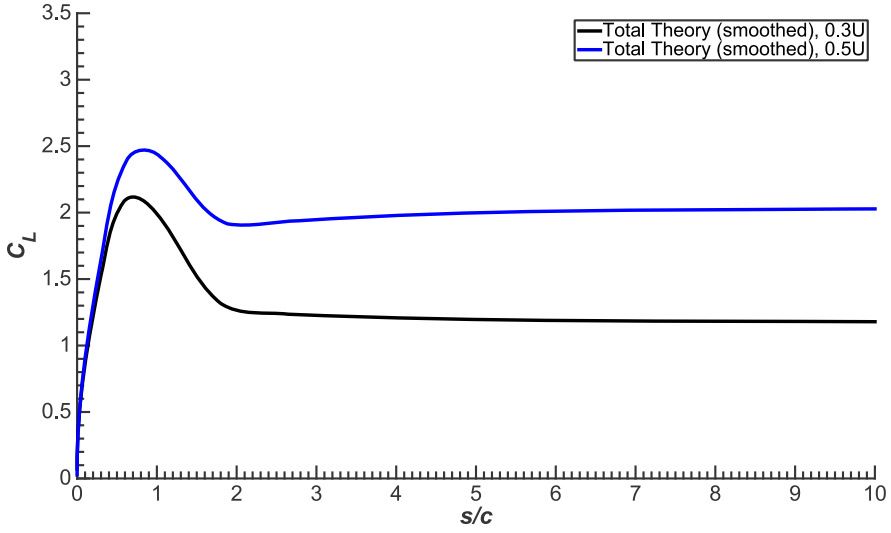

Figure 3-21: Low-Order Model Prediction for Lift Coefficient, for the Fast Surging Case with Two Different Relative LEV-TEV Velocities (All Other Parameters are Unchanged).

Returning to the original model prediction, Figure 3-22 compares the result for the fast surge case to all available datasets. Overall, the agreement is not too bad and the main features of the force history are well captured. The discrepancies during the acceleration period are almost certainly a result of subtly differing kinematics, which, as we have seen, can have a significant impact on the details of the force history at that time.

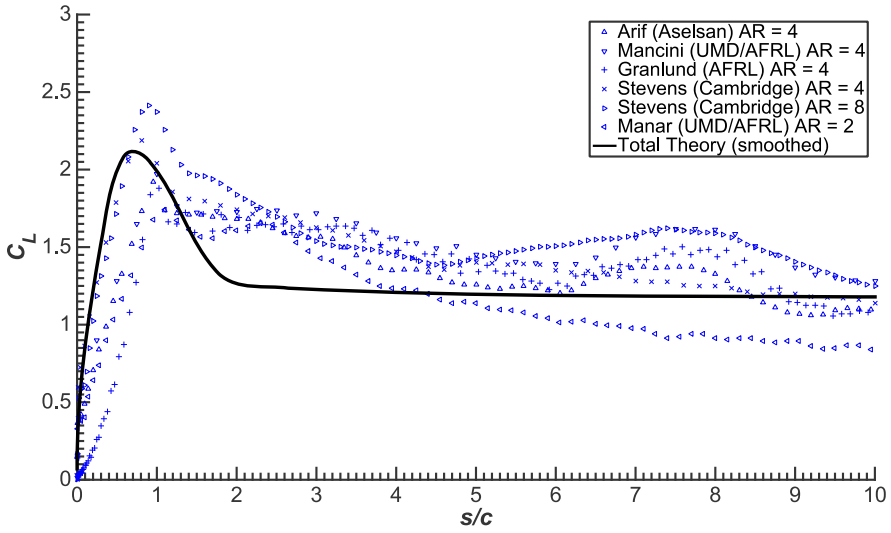

Figure 3-22: Low-Order Model Prediction for the Fast Surging Case, Compared with All Available Data Sets.

Some of the force histories exhibit a small 'second peak' at around eight chords of travel. This is not predicted by the model, and a tentative explanation for its origins is given elsewhere in the Report.

3.4.2 Fast Pitch Case

Next, we turn to the pitch case. The following assumptions are employed:

1) The relative LEV-TEV velocity is set to 0.5 U_∞, in accordance with the recommendations made earlier.
2) The Wagner function is modified by the instantaneous angle of attack during the pitch-up motion.
3) "Eldridge" smoothing is applied in line with the kinematics of the relevant experiment performed by the same group.
4) The distance between any newly formed additional LEV circulation and its TEV counterpart is one chord length (to be used in the 'vortex chord term').

As before, the final model prediction is numerically smoothed to simulate a (small) amount of filtering.

Figure 3-23 shows the Maryland group's prediction for the fast pitch motion. It can be seen that all terms play a significant role during the unsteady part of the cycle and that the subtleties of the force curve are rather well reproduced. It is noteworthy that the model prediction does not display the gradual drop in lift seen later in the motion – this is most likely a result of the gradual drop in the relative TEV-LEV velocity which has not been implemented in the model (recall that at later times 0.3 U_∞ appeared to be a better fit).

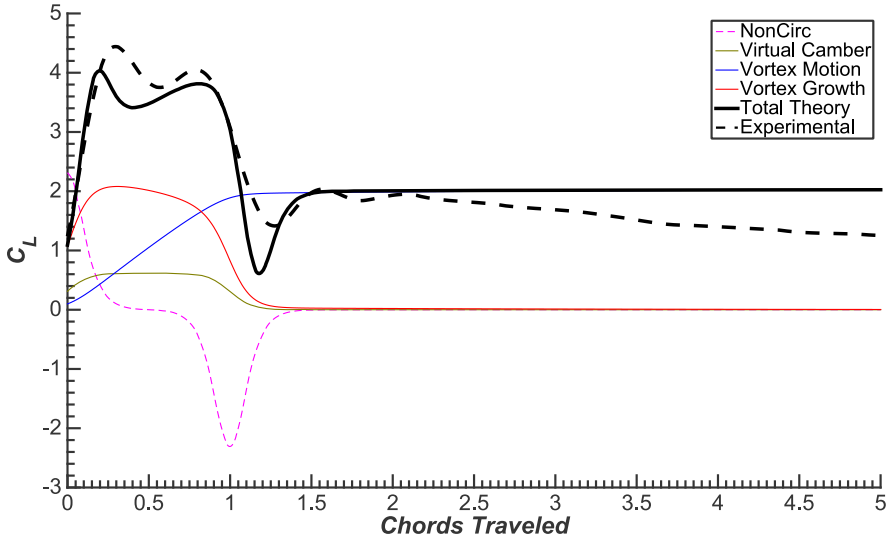

Figure 3-23: Low-Order Model Prediction for the Fast Pitch Case (Maryland Group).

Figure 3-24 shows the prediction for the same motion from Cambridge (albeit with slightly differing 'Eldredge' smoothing [7]). Unsurprisingly, this implementation better fits the Cambridge experimental data (shown in dashed). The large negative spike in the vortex growth term is a result of the apparent drop in effective angle of attack at the end of the motion (when the induced angle of attack vanishes). This has been incorporated in the modification to the Wagner function giving a drop in circulation at this point.

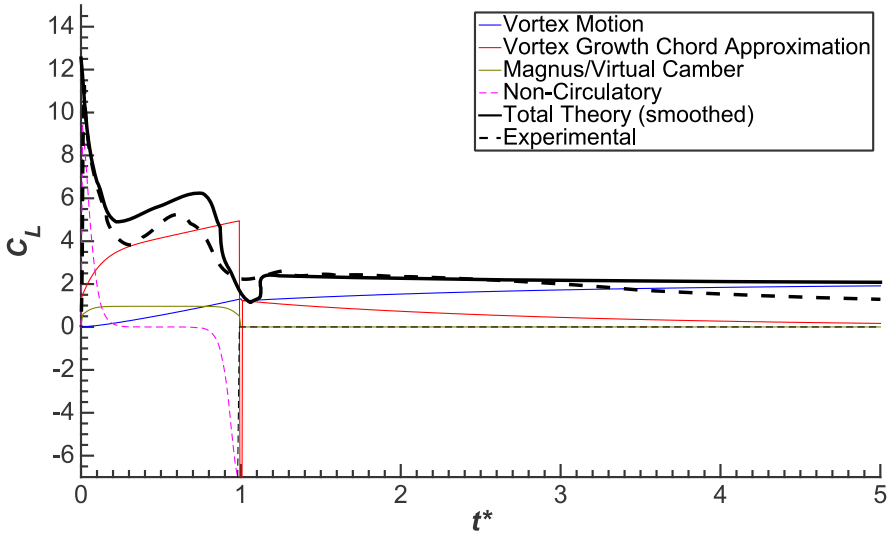

Figure 3-24: Low-Order Model Prediction for the Fast Pitch Case (Cambridge Data).

Finally, Figure 3-25 compares both predictions with all available datasets. It can be seen that both capture the shape of the force curve rather well. There is some over-prediction during the pitch phase, but this may be a result of not capturing the kinematics accurately.

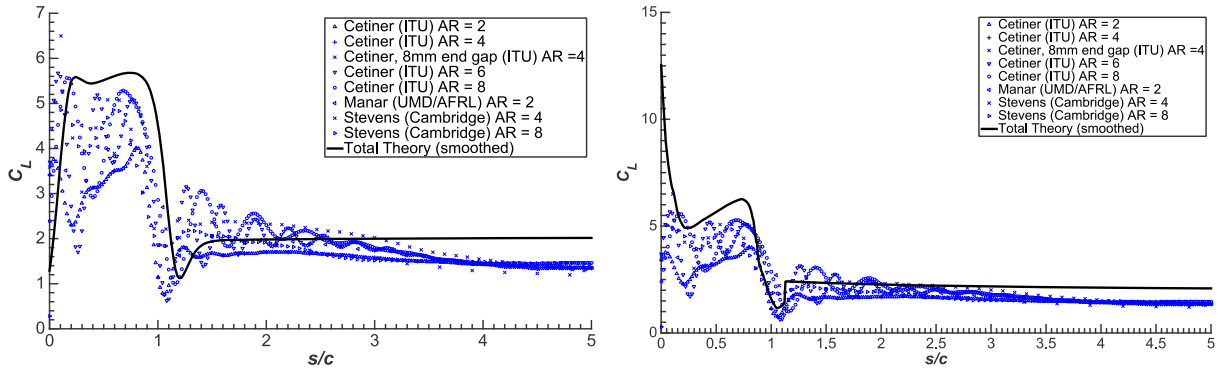

Figure 3-25: Comparison of Low-Order Model's Prediction of Lift Coefficient History vs. that of All Available Data Sets for the Fast Pitching Case.

3.4.3 Slow Pitch and Surge Cases

The model has been found to give a relatively good fit with the data despite the fact that no information on actual vortex strength and motion was used directly (although it did inform the underlying assumptions). Thus, it is worthwhile to apply the same assumptions to the slow cases. It should be emphasized that it was not possible to accurately detect and measure the LEV and it is therefore unknown whether the assumptions of a 'Wagner-like' growth and a simple and constant relative LEV-TEV velocity hold for these cases.

Figure 3-26 shows the model predication for the slow surge case using exactly the same assumptions as for the fast case (modified Wagner vortex growth and 0.3 U_∞ relative LEV-TEV velocity).

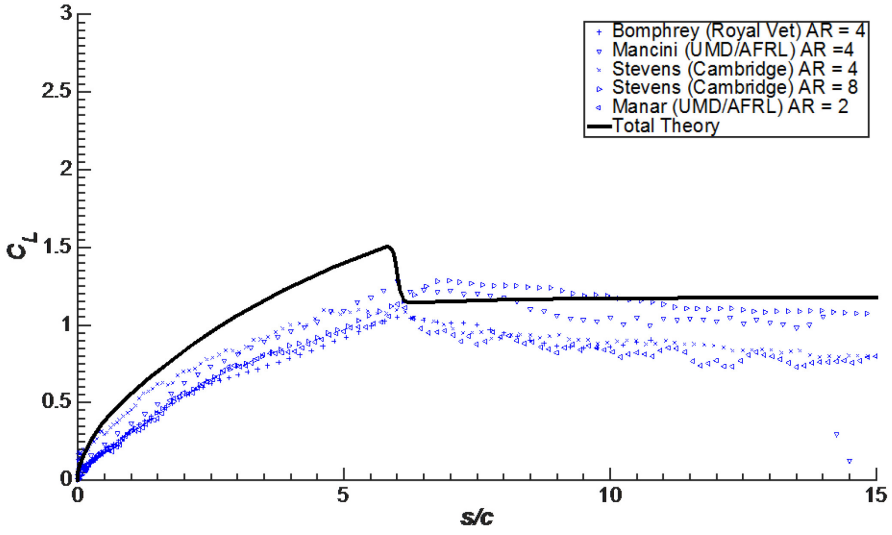

Figure 3-26: Low-Order Model Prediction for the Slow Surging Case.

Given the simplicity of the model, the agreement is satisfactory. Clearly, the vortex growth during the acceleration is over-predicted and this reflects with the experimental observation that no distinct LEV has formed. Nevertheless, the shape of the force distribution and several of its features are well captured.

Using the same model parameters, albeit with an increased LEV-TEV velocity of $0.5\,U_\infty$ (in line with the assumptions made for the fast case), gives the prediction for the pitch case shown in Figure 3-27.

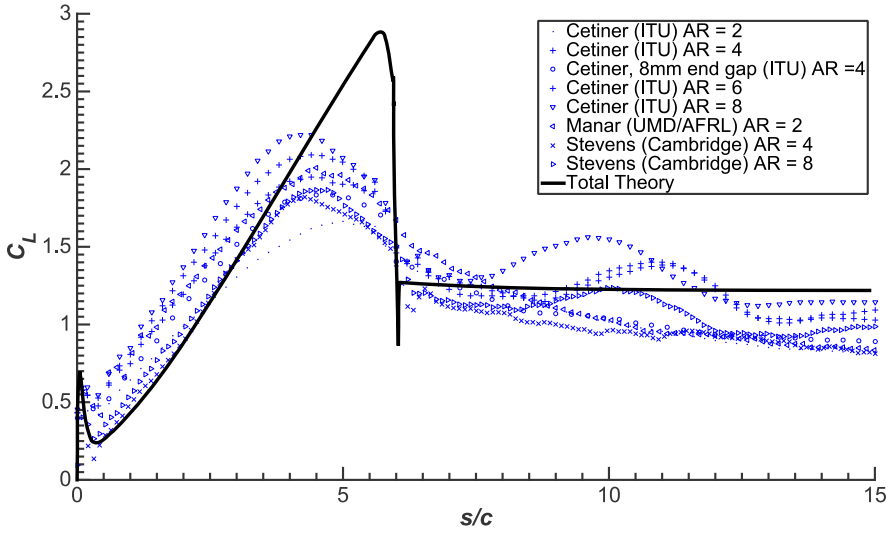

Figure 3-27: Low-Order Model Prediction for the Slow Pitch Case.

Once again, the subtle features of the force history are well captured (note, for example, the small spike at the start of the motion or the gradient of the force distribution during pitch) but the peak in force at the end of the pitch is significantly over-predicted. This is clearly a result of the real flow not being able to sustain a growth in circulation after approximately 3.5 – 4 chords of travel. Close comparison with the flowfields show that this is approximately when the wing becomes stalled, and a large slowly re-circulating wake develops. This raises the question whether the prediction can be improved if this knowledge of 'flow breakdown' is implemented by imposing a maximum on the vortex circulation. This has been done by the Maryland group, and their prediction for the same case is shown in Figure 3-28.

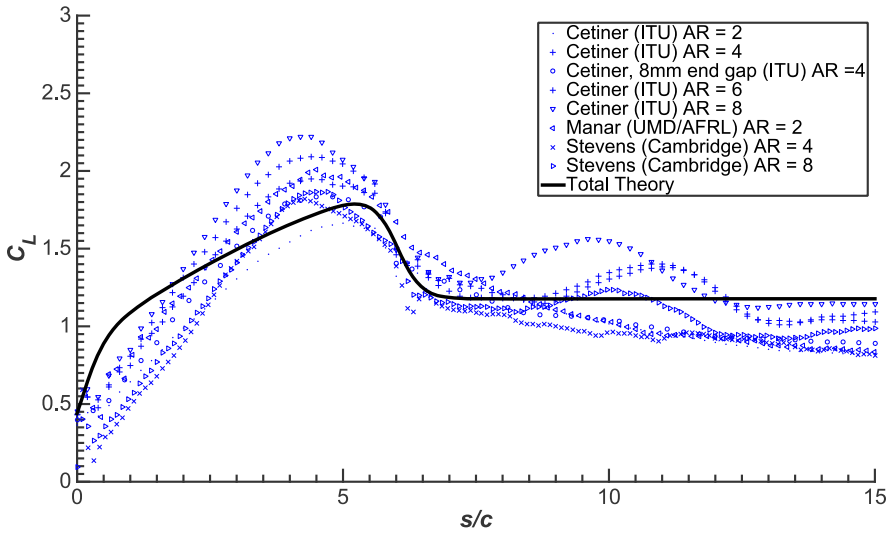

Figure 3-28: Low-Order Model Prediction for the Slow Pitch Case (Maryland Group).

Similar to before, the Maryland group employed a different treatment of the vortex growth which alters the shape of the force curve during the pitch but the behavior towards the end of the pitch and the maximum force are very well predicted.

These comparisons are not yet entirely satisfactory but it can be concluded the low-order force model is capable of capturing most of the relevant physics and that, after a bit of further research and fine-tuning of some of the underlying assumptions, it should be possible to predict the force history of pitching and surging wings with an engineering level of accuracy.